Investigation of Ni@CoO core-shell nanoparticle films synthesized by sequential layer deposition

M.C. Spadaro[1,2], P. Luches[2], F. Benedetti[1,2], S. Valeri[1,2], S. Turchini[3], G. Bertoni[4], A. M. Ferretti[5], E. Capetti[5], A. Ponti[5], S. D'Addato[1,2*]

[1]CNR-NANO, via G. Campi 213/a, 41125 Modena, Italy.

[2]Dipartimento FIM, Università di Modena e Reggio Emilia, via G. Campi 213/a, 41125 Modena, Italy.

[3]CNR-ISM, Via Fosso del Cavaliere 100, 00133 Roma, Italy

[4]CNR-IMEM, Parco Area delle Scienze 37/a - 43124 Parma, Italy

[5]Laboratorio di Nanotecnologie, Istituto di Scienze e Tecnologie Molecolari, Consiglio Nazionale delle Ricerche, via G. Fantoli 16/15, 20138 Milano, Italy

Films of Ni@CoO core-shell nanoparticles (NP Ni core size $d \approx 11$ nm) have been grown on Si/SiO_x and lacey carbon supports, by a sequential layer deposition method: a first layer of CoO was evaporated on the substrate, followed by the deposition of a layer of pre-formed, mass-selected Ni NPs, and finally an overlayer of CoO was added. The Ni NPs were formed by a magnetron gas aggregation source, and mass selected with a quadrupole mass filter. The morphology of the films was investigated with Scanning Electron Microscopy and Scanning Transmission Electron Microscopy. The Ni NP cores have a shape compatible with McKay icosahedron, caused by multitwinning occurring during their growth in the source, and the Ni NP layer shows the typical random paving growth mode. After the deposition of the CoO overlayer, CoO islands are observed, gradually extending and tending to merge with each other, with the formation of shells that enclose the Ni NP cores. In situ X-ray Photoelectron Spectroscopy showed that a few Ni atomic layers localized at the core-shell interface are oxidized, hinting at the possibility of creating an intermediate NiO shell between Ni and CoO, depending on the deposition conditions. Finally, X-ray Magnetic Circular Dichroism at the Ni $L_{2,3}$ absorption edge showed the presence of magnetization at room temperature even at remanence , revealing the possibility of magnetic stabilization of the NP film.

Keywords: Ni, CoO, core-shell nanoparticles, electron microscopy, X-ray photoelectron spectroscopy, X-ray magnetic circular dichroism

Introduction

Research on metal/oxide core-shell nanoparticles (NPs) is a major area of interest in material science because of the fundamental role of these materials in magnetic recording, catalysis, nanomedicine, and photovoltaics [1, 2]. In the past years, great attention has been devoted to design smart strategies to overcome the superparamagnetic (SPM) limit, which affects magnetic stability in NPs at room temperature (RT) and hampers the possibility of reducing the size of memory units [3, 4]. For instance, it can be easily estimated that a Ni NP with a diameter $d \approx 34$ nm (corresponding to a volume $V = 2.1 \cdot 10^4$ nm^3) has a blocking temperature $T_B = 300$ K, by using the formula $T_B = KV/25k_B$ and Ni anisotropy constant $K = 0.5 \cdot 10^4$ J/m^3 [5]. The Exchange Bias (EB) effect can be of help in tackling this problem: in fact, the exchange interaction at the interface between an antiferromagnetic (AFM) and a ferromagnetic (FM) material induces an additional unidirectional magnetic anisotropy, leading to the well-known shift of the hysteresis loop. In this way, the EB can pin the spins in the FM material and stabilize their alignment along a magnetically pre-definite direction, increasing the magnetization stability [2,6]. This effect was exploited in core-shell NPs with a FM metal core and an AFM oxide shell, like Co@CoO and Ni@NiO systems [2, 4, 7, 8]. In the case of Co@CoO NP films, it was found that T_B, coercivity, and the EB field increase with the NP areal density, due to a modification of the magnetic properties caused by the neighboring oxide shells coming into contact, and providing a more efficient exchange interaction with the FM cores [3, 4].

The control of the AFM/FM exchange coupling is a difficult task, because it depends on the structural details of the interface, and on the morphological, electronic, and magnetic properties of both the core and the shell. Some degree of tunability of the exchange coupling can only be achieved by a careful control of the NP synthesis and, consequently, of the NP physical properties (core/shell structure, shell thickness, oxide composition, and interface quality). Several methods have been used to synthesize metal/metal-oxide core/shell NPs: wet chemical synthesis, lithography, self-assembly, physical vapor deposition, and thermally assisted precipitation in a

matrix [8-12]. The formation of oxide shells was generally obtained by oxidation of the metallic NP cores. This method was applied to Co@CoO [2,3] and Ni@NiO systems [13,14]. Physical synthesis obtained by evaporation and NP aggregation with noble gas carriers presents the advantage of a clean environment, which allows for the production of samples free of organic ligands [15-19]. Evaporation realized with a DC magnetron source also allows a good control over the NPs size and dispersion, by a careful adjustment of many parameters, namely the magnetron discharge power, the length of the aggregation region and the carrier gas flow [15]. Recently, this method was implemented with co-deposition : a separate evaporator, like for instance a thermal molecular beam epitaxy (MBE) source in the experimental chamber generates a beam of atoms that can form shells around the pre-formed NPs while they are being deposited on the substrate. Alternatively, in the so-called sequential layer deposition mode, the NP can be embedded within two layers evaporated by MBE. The shells can be made of either metals or oxides, if the co-deposition is performed in oxygen atmosphere [7, 20-22]. By this method it was possible to perform a systematic and accurate investigation of the morphology, structure and magnetic properties of Ni@NiO core-shell NPs by a number of different techniques [7]. Details about the FM/AFM interface structure were revealed and related to the presence of EB effects in the NP assemblies. Moreover, tuning of the EB was achieved by changing the thickness of the NiO shell while keeping the Ni core size fixed, at variance with previous experiments where the shell was grown at the expenses of the metallic core [20]. In principle, non-native metal oxide shells can be grown in this way, widening the range of metal/oxide core/shell systems amenable to investigation and optimization [19, 21, 22]. From this point of view, a promising system is Ni@CoO NPs. In fact, the Ni/CoO interface is expected to be (at best) of similar quality to the Ni/NiO interface (cell size: a_{Ni} = 0.352 nm, a_{NiO} = 0.418 nm, a_{CoO} = 0.426 nm), but CoO has a much larger antiferromagnetic anisotropy than NiO ($K_{CoO}/K_{NiO} \cong 10^7$), which is expected to induce a substantial increase in EB and coercive field. On the basis of the previous considerations, it was natural to exploit the sequential layer deposition technique to obtain films of Ni@CoO NPs. The present work reports the results

obtained on Ni@CoO NP assemblies, in terms of interfacial morphology and oxidation state of interface ions, in order to optimize the parameters governing the NP growth. The used techniques were X-ray Photoelectron Spectroscopy (XPS), Scanning Electron Microscopy (SEM) and Scanning Transmission Electron Microscopy (STEM). X-ray Magnetic Circular Dichroism (XMCD) at the Ni $L_{2,3}$ absorption edge was used to study the Ni magnetic moment under an applied magnetic field and at remanence. In a previous study Ni@CoO NPs assemblies were realized by using a combination of thermal evaporation (for Ni cores) and laser ablation (for CoO shells) followed by inert gas condensation [19]. The layered structures were collected and analyzed *ex-situ* by XPS, XRD, TEM and SQUID magnetometry. In that case the shell around the Ni NPs comprised an inner NiO layer and an outer Co_3O_4 layer. EB was observed up to T= 45 K, a temperature similar to the Neèl temperature of Co_3O_4. On the other hand, realization of Ni@NiO systems obtained with the sequential layer deposition demonstrated the possibility to tune EB by the fine regulation of a "bulk" parameter, such as the AFM anisotropy, which was obtained by changing the thickness of the NiO shells, without modifying the size of the Ni cores [7, 20]. At variance with the work described in ref. [19], in which the experimental results were reported only for NPs with one specific size value for the core diameter and the shell thickness, the present study is focused on controlling the procedure of shell formation. Moreover, it discusses the evolution of the NP film morphology for different shell thickness, and it correlates the magnetic properties of the system with the chemistry of the core/shell interface region.

Experimental

The NP assemblies were grown in an experimental system consisting of three interconnected vacuum chambers [23]. The substrates used were p-doped Si (100) wafers with its native oxide (Si/SiO_x) for XPS, SEM, and XMCD analysis, and lacey C-coated copper grids for STEM measurements. A beam of pre-formed Ni NPs was created in a gas-aggregation magnetron source (nanocluster source NC200U, Oxford Applied Research: magnetron discharge power P = 35 W,

and Ar flow f = 50 sccm) and mass-selected with a quadrupole mass filter (QMF), as approximately 90% of the NPs obtained from the source were electrically charged. In these conditions we could obtain Ni NPs with a linear size distribution between 8 and 15 nm and average diameter $<d>$=11 nm, as directly verified by analyzing the SEM images [7, 20]. The NP beam impinged on the substrate in a chamber with base pressure p=7 $\cdot 10^{-9}$ mbar, that increased to $p \approx 10^{-4}$ mbar during deposition, because of the presence of Ar gas carrier in the source. A MBE evaporator was used for the deposition of Co in the presence of O_2, which was introduced in the deposition chamber through a leak valve. The partial oxygen pressure varied between $p_{O2} = 5 \cdot 10^{-8}$ and $2 \cdot 10^{-7}$ mbar. The samples were prepared in three steps:

1) Reactive deposition of the first CoO layer with nominal thickness t^1_{CoO} = 1 nm.
2) Deposition of a layer composed of Ni NPs; the amount of deposited Ni, expressed in terms of nominal thickness, was t^2_{Ni} = 6 nm. This quantity corresponds to the thickness of a continuous film of bulk Ni, with the same mass as the amount of deposited Ni NPs. It was estimated that a single layer of close-packed Ni equal spheres with d=11 nm has the same mass as a continuous film with t^2_{Ni} = 6 nm.
3) Reactive deposition of a CoO overlayer, with variable nominal thickness t^3_{CoO} = 0.5 - 6 nm.

The first CoO layer was deposited in order to have a Ni/CoO interface beneath Ni, thus completing the CoO shells around the deposited Ni NPs. The amount of deposited material was checked with a quartz microbalance, and after each deposition step the sample was transferred *in vacuo* to the analysis chamber, equipped with an Al-Mg twin anode X-ray source (XR50, Specs), generating Mg K_α photons (hv = 1253.6 eV), and an electron hemispherical analyzer (Phoibos 150, Specs) for *in situ* XPS analysis [18].

SEM images were acquired with a Nova Nano SEM450 (FEI Company-Bruker Corporation). The SEM column is equipped with a Schottky field-emission gun (SFEG) and it can achieve a resolution of 1.4 nm in low-voltage (1 KV) operation. The STEM experiments were performed using a JEOL JEM-2200FS microscope equipped with a Schottky field-emission gun working at 200 KeV. The

instrument has an objective lens spherical aberration coefficient of 0.5 mm, permitting a point-to-point resolution of 0.19 nm. Some samples were also packed in nitrogen atmosphere and transferred to the CiPo beamline at ELETTRA, Trieste [24], for XMCD measurements at the Ni $L_{2,3}$ edge. XMCD absorption spectra were obtained by measuring the drain current from the samples at a glancing angle $\Theta = 20°$, after field cooling in the presence of a magnetic field H= 0.3 KOe down to T=5 K, with H forming an angle of 20° with the sample surface. In this way, it was possible to probe the component of the magnetic moment parallel to the sample surface. The measurements were performed at RT after field cooling at T=5 K, both in the presence of a magnetic field H=0.3 KOe and in remanence conditions (H = 0), with left-handed and right-handed circularly polarized radiation.

Results and discussion

The Ni@CoO films have been investigated with SEM and STEM, in order to understand their growth morphology. Fig. 1(a)-(c) are SEM images of three different films, in which the thicknesses of the first layer of CoO and the amount of Ni NPs were kept fixed (t^1_{CoO} = 1 nm, t^2_{Ni} = 6 nm), while the thickness of the overlayer was varied, amounting to t^3_{CoO} = 1, 3.5 and 6 nm, respectively. In all images, the granular structure of the films is very clear, and the resulting morphology is similar, as the NP film grows according to the random paving mode [18]. By looking more carefully at the images in Fig. 1(a) and (b), it can be observed that some smaller grains appear on the NPs at increasing coverage of the CoO overlayer. The small grains, which are not present on the Ni NPs prior to the deposition of the oxide, are due to the formation of CoO islands that tend to cover the NPs, forming a shell, in analogy with Ni@NiO NPs prepared by the same method [7]. In some cases the NPs appear to merge, as these growing islands extend also between neighboring NPs.

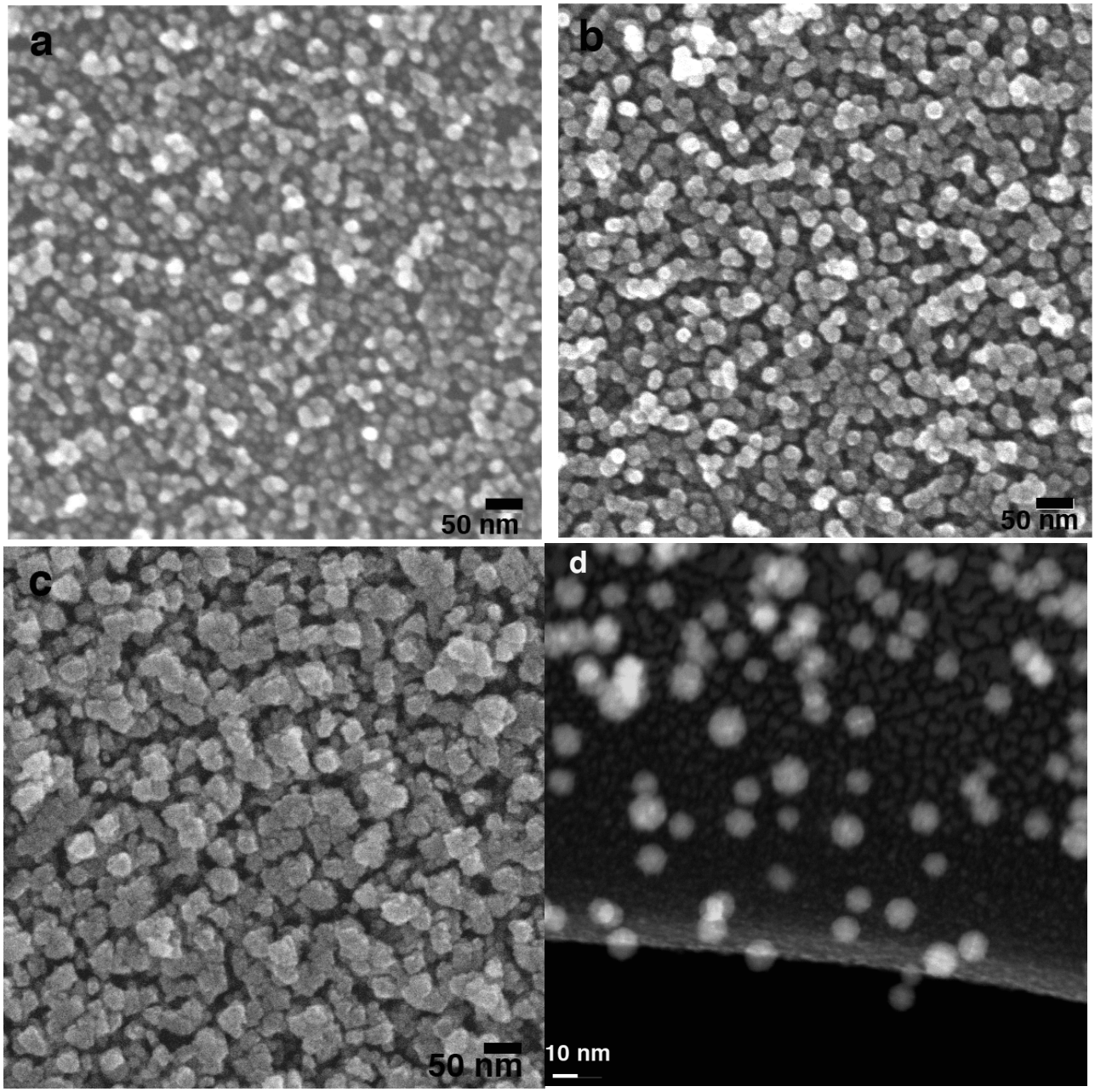

Fig. 1. SEM images of Ni@CoO NP films obtained with at increasing coverage of the second CoO layer thickness: (a) t^3_{CoO}=1 nm, (b) t^3_{CoO}=3.5 nm, (c) t^3_{CoO}=6 nm. (d) STEM image of Ni@CoO NPs deposited on a Lacey carbon grid, with t^1_{CoO}= 1nm, t^2_{Ni} = 1nm and t^3_{CoO} = 2 nm.

In the SEM image of Fig. 1(c) structures larger than individual NPs can be seen, with linear size between 15 and 50 nm, which we interpreted as CoO shells extending over several Ni NPs. The approximately square-like shape of these structures is probably due to formation of crystalline CoO nanocubes. Better resolved images could be obtained with STEM. In this case, the amount of bare

Ni NPs correspond to nominal t^2_{Ni}=1 nm, while the thicknesses of the bottom and top CoO layers were t^1_{CoO} = 1nm and t^3_{CoO} = 2 nm, respectively. The STEM image in Fig. 1(d) was taken close to a hole in the C film support (characteristic of the lacey type support used in the experiment) with some NPs partially suspended over the hole. On the carbon support, single NPs lie on the first CoO layer, which has the form of a "percolated" film, due to the coalescence of CoO islands during the growth process. The Ni cores present a regular shape, namely McKay icosahedral shape [24], as already observed for Ni [22,25] and for other fcc transition metals and alloys [21,26, 27]. The McKay icosahedra are due to multitwinning occurring during the NP growth in the source, and they consist of fcc Ni tetrahedral crystallites with slightly distorted (111) facets [26-28]. Some smaller grains appear on the NPs surfaces, which are an indication of the growth of CoO islands during the deposition of the CoO overlayer. This evidence for the Ni NP core structure was not observed in high resolution TEM results reported in ref. [19]. A possible explanation could be that the parameters governing the NP growth in the two experiments are different. In our case, "freezing" during the growth process causes the formation of a metastable icosahedral structure [26-29].

In order to collect information about the oxidation state of the Ni and Co atoms in the films, *in situ* XPS spectra were taken after each deposition procedure, focusing on the Ni 2p core level emission. Co 2p spectra were also taken after the completion of the first and of the top CoO layers, and the same line shape, characteristic of bulk CoO, was observed in all the samples. Ni 2p spectra taken after the deposition of Ni NPs showed features characteristic of the metallic state, as observed in previous experiments on similar systems [7, 21, 23]. After depositing the top layer of CoO, the Ni 2p spectra showed a different shape, caused by the presence of an extra component, ascribed to oxidized Ni. As an example, the spectra reported in Fig. 2 were taken after the growth of the top CoO layer on three samples (named here A, B and C), using different deposition parameters (partial oxygen pressure, deposition time and Co evaporator power, see Table 1). A de-convolution of the Ni 2p spectra into a metallic Ni and an oxidized Ni component was performed to estimate the

amount of oxidized Ni,, using the method described in ref. [30].

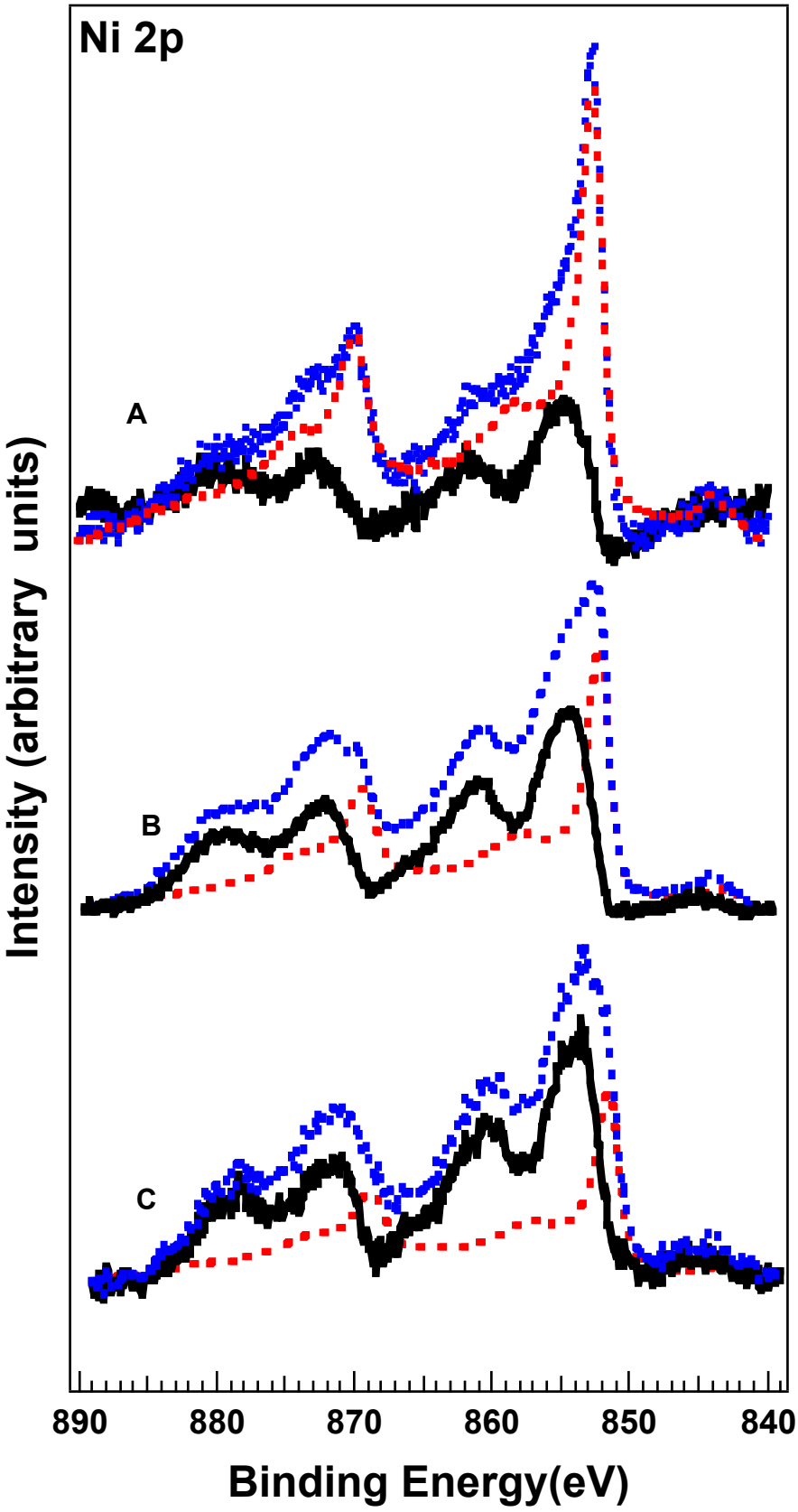

Fig. 2. Ni 2p core level XPS spectra and de-convoluted components of Ni@CoO NP films, with the top CoO layer grown in different experimental conditions. Blue dotted line: total spectrum. Red

dashed line: metallic component. Black continuous line: oxidized component. Spectra were taken from three samples (A, B, C) prepared using different values of the growth parameters for the top CoO layer.

A Shirley background and a spectrum of metallic Ni (recorded from a bare Ni NP film) [23] with variable weight were subtracted from the spectra recorded after the deposition of the CoO overlayer, to obtain approximately the contribution of the oxidized Ni fraction to the XPS lineshape. The criterion used to estimate the relative weight of the metallic contribution was to subtract the largest metallic Ni spectral component, provided that the intensity in the energy region between 845 and 890 eV remained non negative [23, 30]. The lineshape of the component assigned to the oxidized Ni is very similar to that observed in NiO. However a broad, intense peak located at binding energy E_b= 855 eV, corresponding to photoexcitation from Ni $2p_{3/2}$ core level is observed, instead of the two features typical of stoichiometric NiO, which are respectively at E_B=853.5 eV and 856 eV [23, 30]; this finding suggests that Ni atoms are not completely coordinated with the six nearest neighbour O atoms, like in rock salt NiO [30], possibly because of a large number of defects and/or local lattice distortion in this layer. The de-convolution analysis allowed to obtain also the area of the oxidized component A_{NiO}, normalized to the area of the total spectrum (A_{tot}), as reported in Table 1. The A_{NiO}/A_{tot} ratio found for the three samples varies between 0.45 and 0.64, but these values largely overestimate the real amount of oxidized Ni. In fact, the photoelectron escape depth λ has to be taken into account, which can be estimated at $\lambda \approx$ 1.0 nm for Ni 2p photoelectrons having kinetic energy $E_k \approx$ 400 eV. As a gross approximation, the NP can be modeled as a spherical metallic Ni core with concentric NiO and CoO shells. Therefore, the photoelectrons coming from the Ni core travel through part of the core (depending on the depth of the site where the primary ionization process occurs) and both NiO and CoO shells, while photoelectrons from oxidized Ni travel through part of the NiO shell and the whole CoO shell. The method developed by Shard [31] was used, in order to estimate the thickness of the oxidized Ni shell, d_{NiO}, reported in Table 1. It can be observed that the values of d_{NiO} obtained for the three samples range between 0.3 nm and 0.6 nm. These values correspond to *ca.* 1 - 1.5 NiO crystal cells (a_{NiO} =0.417 nm). It is therefore reasonable to deduce that when the CoO shell is formed, the two (samples A and B) or three (sample C) outmost atomic layers of the Ni core are oxidized. It is expected that the presence of this interfacial region affects the exchange coupling between the AFM shell and the FM core. The method used here to synthesize Ni@CoO NPs is similar to previous works on Ni@MgO [20], FePt@MgO [21] and Ni@NiO [7, 19] NP films. In all cases, the oxide shell did not modify the original structure of the multitwinned core. Interestingly, XPS data did not reveal the formation of oxidized Ni in

Ni@MgO [20]. The reason may be ascribed to the lower electronegativity of Mg (1.31 Pauling) with respect to Ni (1.91 Pauling), which favors the oxidation of Mg. In FePt@MgO NPs, some oxidation of Fe was deduced from Fe 2p XPS analysis, while the Pt 4f spectra remained unchanged. The different electronegativity values of Fe (1.83 Pauling) and Pt (2.28 Pauling) can again explain this behavior. The formation of a thin shell of NiO between Ni and CoO is similar to what previously observed by Ceylan *et al.* [19], that was ascribed to the similar electronegativity values of Ni and Co (1.88 Pauling). Our NPs are however different from those previously obtained under several respects. In the present case the Ni cores are larger (11 nm *vs.* 5 nm), the shell is composed of pure CoO (in contrast, the shells observed in the work reported in [19] were composed of Co_3O_4 and Co suboxides), and in our case the feasibility of controlling the CoO shell thickness was demonstrated.

Sample	**t^3_{CoO} (nm)**	**Deposition Time (min)**	**P_{o2} (mbar)**	**Evaporator Power (W)**	**A_{NiO}/A_{tot}**	**d_{NiO} (nm)**
A	1.8	420	$5.0 \cdot 10^{-8}$	89.3	0.45±0.05	0.3±0.1
B	1.0	240	$1.6 \cdot 10^{-7}$	90.4	0.52±0.05	0.4±0.1
C	1.0	75	$1.9 \cdot 10^{-7}$	138.3	0.64±0.05	0.6±0.1

Table 1. Experimental condition parameters for three Ni@CoO films, with relative XPS intensity component of oxidized Ni and thickness of NiO shell estimated by the Shard model [31].

Finally, XMCD experiments were carried out on some Ni@CoO NP films. Fig. 3 shows Ni $L_{2,3}$ XMCD spectra taken at RT, under an applied field H=0.3 kOe and at remanence (H=0) for a NP film with t^3_{CoO}= 1 nm. The difference between spectra taken with right-handed and left-handed circularly polarized light shows evidence of dichroism in both cases. This result suggests the presence in the NP film of a remanent magnetization, at variance with the case of bare NPs, which are in the SPM state at RT, with some coupling due to exchange and magnetostatic interaction, as previously shown [18]. A SPM phase at RT was observed also on Ni/NiO/CoO NPs in ref. [19]. A possible explanation for this different behavior would lie in the different values of the core diameter sizes, together with a different interface structure due to the growth conditions. A larger core size

would give a larger magnetic anisotropy energy, with a stable state induced by the AFM/FM interface coupling at higher temperature. The dichroism values obtained at the L_3 edge are respectively D= 0.16 for H=0.3 KOe and D=0.05 at H=0, where $D = (I^+(L_3) - I^-(L_3))/I(L_3)$, I^+, I^- are the absorption intensity values with right-handed and left-handed polarization, and I is the average of I^+ and I^- . An estimate of the average magnetic moment per Ni atom $\langle m \rangle$ was obtained by applying the sum rules [32] to the difference spectra reported in Figure 3. By assuming a degree of circular polarization P=0.8, it was found $\langle m \rangle \approx 0.35 n_h$ μ_0/atom for H=0.3 kOe and $\langle m \rangle \approx 0.23$ n_h μ_0/atom for H=0, where n_h is the number of holes in the Ni d-band and μ_0 is the Bohr magneton. There is some uncertainty about the value of n_h, which has been estimated to be between 1.5 and 1.78 [33]. Even with n_h = 1.78, the obtained values for $\langle m \rangle$ are $\langle m \rangle \approx 0.61$ μ_0/atom for H=0.3 kOe and $\langle m \rangle \approx 0.41$ μ_0/atom for H=0. These values are smaller than the value for bulk Ni (m=0.69 μ_0/atom) [34]. The reason for these discrepancies could be that the film has not reached saturation under the used experimental conditions. This is supported by our previous observation on Ni NPs with $\langle d \rangle$ = 12 nm. In that case the Ni NPs reached magnetic saturation beyond 0.3 kOe, while bare NPs on 1 nm thick NiO layer saturated at ca. 1 kOe, and Ni@NiO core@shell NPs saturated at 1.5 – 2 kOe) [7]. Nevertheless, the presence of dichroism at RT suggests a stabilization of the NPs caused by the presence of the AFM CoO shells.

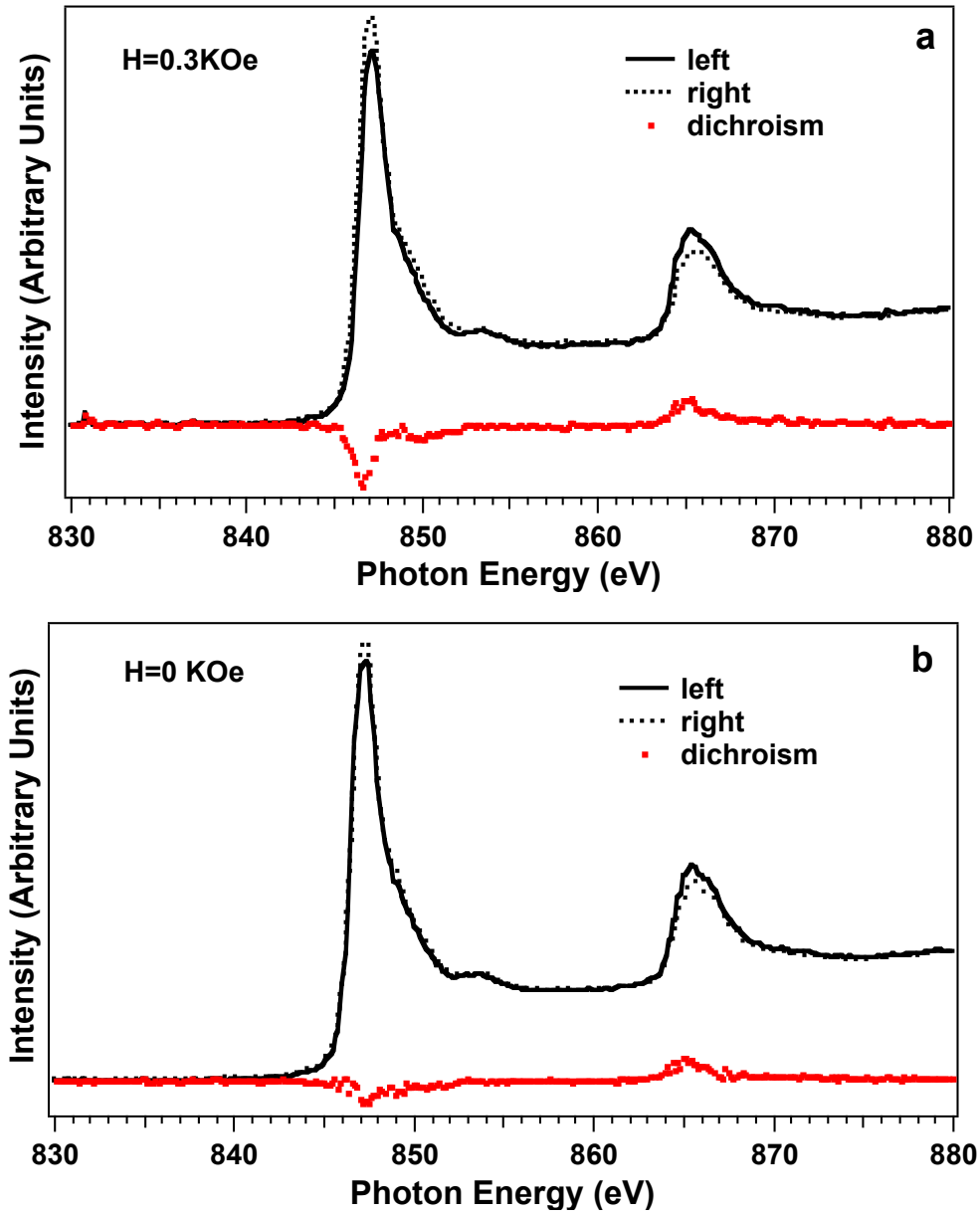

Fig. 3. Ni $L_{2,3}$ edge XMCD spectra taken from Ni@CoO NP, with t^3_{CoO} = 1 nm at room temperature with (a) H=0.3 kOe and (b) in remanence conditions.

Conclusions

Films of Ni@CoO core-shell NPs grown on Si/SiO_x were successfully obtained with sequential layer deposition, by depositing a first layer of CoO, a layer of preformed, mass-selected Ni NPs obtained by a magnetron gas-aggregation source, and an overlayer of CoO. SEM and STEM images

show the growth of a discontinuous CoO first layer, where the NPs are adsorbed. At increasing Ni amount, the NP film follows the random paving growth mode. STEM images are compatible with Ni cores having a McKay icosahedron shape, due to multitwinning that occurs during the formation of the NPs in the source. When the top CoO layer is deposited, small islands grow, and at increasing CoO amount the islands tend to cover the whole NPs, even extending to neighboring NPs and merging with them. From the XPS analysis, it was found that most of the Ni core remains in the metallic state after the second CoO deposition. Some Ni was oxidized at the core-shell interface, and an analysis of the intensity of Ni 2p components allowed us to estimate the thickness of this oxidized Ni shell between 0.3 and 0.6 nm, whule the core diameter is about 11 nm. This interface layer may play an important role in the exchange coupling between the FM Ni core and the AFM CoO shell. Finally, the presence of magnetic dichroism at RT – even at remanence – suggests pinning of the NP magnetic moments and stabilization induced by the AFM CoO shell.

Acknowledgements.

This work has been supported by the Italian MIUR through the FIRB Project RBAP115AYN, "Oxides at the nanoscale: Multifunctionality and applications". Elettra infrastructure is acknowledged for providing access to synchrotron radiation. M. Zapparoli is acknowledged for assistance in SEM measurements.

References

[1] R. Hao, R. Xing, Z. Xu, Y. Hou, S. Gao, S. H. Sun, Adv. Mat. **22** (2010) 2729.

[2] J. Noguès, J. Sort, V. Langlais, V. Skumryev, S. Suriñaz, J. S. Muñoz, M. D. Barò, Phys. Rep. **422** (2005) 65.

[3] V. Skumryev, S. Stoyanov, Y. Zhang, G. Hadjipanayis, D. Givord, J. Nogués, Nature **423** (2003) 850.

[4] J. Nogués, V. Skumryiev, J. Sort, S. Stoyanov, D. Givord, Phys. Rev. Lett. **97** (2006) 157203.

[5] D. Jiles, "Magnetism and Magnetic Materials", 1998, Chapman and Hall, London.

[6] C. P. Beans, J. D. Lingston, J. Appl. Phys. **30** (1959) 1205'

[7] M. C. Spadaro, S. D'Addato, P. Luches, S. Valeri, V. Grillo, E. Rotunno, M. A. Roldan, S. J. Pennycook, A. M. Ferretti, E. Capetti, A. Ponti, Nanotechnology **26** (2015) 405704.

[8] S. H. Sun, C. B. Murray, D. Weller, L. Folks, A. Moser, Science **287** (2000) 1989.

[9] S. H. Sun, C. B. Murray, J. Appl. Phys. **85** (1999) 4325.

[10] J. I. Martìn, J. Nogués, K. Liu, J. L. Vicent, I. K. Schuller, J. Magn. Magn. Mater. **256** (2003) 449.

[11] S. D'Addato, R. Gunnella, F. Borgatti, R. Felici, P. Finetti, Surf. Sci. **601** (2007) 329.

[12] P. Allia, M. Coisson, F. Spizzo, P. Tiberti, F. Vinai Phys. Rev. B **73** (2006) 054409.

[13] J. B. Yi, J. Ding, Z. L. Zhao, B. H. Liu J. Appl. Phys. **97** (2005) 10K306.

[14] A. C. Johnston-Peck, J. Wang and J. B. Tracy ACS Nano **3** (2009) 1077.

[15] J. Meldrim, Y. Qiang, Y. Liu, H. Haberland, D. J. Sellmyer, J. Appl. Phys. **87** (2000) 7013.

[16] C. Binns, K. N. Trohidou, J. Bansmann, S. H, Baker, J. A. Blackman, J. –P. Bucher, D. Kechrakos, A. Kleibert, S. Louch, K. –H. Meiws-Broer, G. M. Pastor, A. Perez, Y. Xie, J. Phys. D: Appl. Phys. **38** (2005) R357.

[17] A. Kleibert, J. Passig, K. –H. Meiwes-Broer, M. Getzlaff, J. Bansmann, J. Appl. Phys. **101 (**2007) 114318.

[18] S. D'Addato, L. Gragnaniello, S. Valeri, A. Rota, A. di Bona, F. Spizzo, T. Panozaqi, S. F. Schifano, J. Appl. Phys. **107** (2010) 104318.

[19] A. Ceylan, A. K. Rumaiz, S. Ismath Sha, J. Appl. Phys. **101** (2007) 094302.

[20] S. D'Addato, M.C. Spadaro, P. Luches,V. Grillo, S. Frabboni, S. Valeri, A. M. Ferretti, E. Capetti, A. Ponti, Appl. Surf. Sci **306** (2014) 2.

[21] S. D'Addato, V. Grillo, S. Altieri, S. Frabboni, F. Rossi and S. Valeri, J. Phys. Chem. C **115** (2011) 14044.

[22] S. D'Addato, V. Grillo, A. di Bona, S. Frabboni, S. Valeri, P. Lupo, F. Casoli and F. Albertini Nanotechnology **24** (2013) 495703.

[23] S. D'Addato, V. Grillo, S. Altieri, R. Tondi, S. Valeri, S. Frabboni, J. Phys.: Condens. Matter **23** (2011) 175003.

[24] D. Desiderio, S. Difonzo, B. Diviacco, W. Jark, J. Krempasky, R. Krempaska, F. Lama, M. Luce, H. C. Mertins, M. Placentini, T. Prosperi, S. Rinaldi, G. Soullié, F. Schäfers, F. Schmolle, L. Stichauer, S. Turchini, R. P. Walker, and N. Zema, Synchr. Rad. News **12**, 34 (1999).

[25] A. L. Mackay, Acta Cryst. **15** (1962) 916.

[26] S. D'Addato, V. Grillo, S. Altieri, S. Frabboni, S. Valeri, Appl. Surf. Sci. **260** (2012) 13.

[27] R. Wang, O. Dmitrieva, M. Farle, G. Dumpich, M. Acet, S. Mejia-Rosales, E. Perez-Tijerina, M. J. Yacaman, C. Kisielowski, J. Phys. Chem. C **113** (2009) 4395.

[28] C. L. Johnson, E. Snoeck, M. Ezcurdia, B. Rodrìguez-Gonzàlez, J. Pastoriza-Santos, R. M. Liz-Marzan, M. J. Hÿtch, Nature Mat. **7** (2008) 120.

[29] S. Ino, J. Phys. Soc. Jpn. **27** (1969) 941.

[30] C. Giovanardi, A. di Bona, S. Valeri, (2004) Phys. Rev. B **69** (2004) 075418.

[31] A. G. Shard, J. Phys. Chem C **116** (2012) 16806.

[32] C. T. Chen, Y.U. Idzerda, H.-J. Lin, N. V. Smith, G. Meigs, E. Chaban, G. H. Ho, E. Pellegrin, F. Sette, Phys. Rev. Letters **75** (1995) 152.

[33] J. Stöhr, H. C. Siegmann, Magnetism from fundamentals to nanoscale dynamics, 2005 Springer, Berlin.

[34] J. Stöhr, J. El. Spec. Rel. Phen. **75** (1995) 253.